IEEE Access
Multidisciplinary | Rapid Review | Open Access Journal

Date of publication xxxx 00, 0000, date of current version xxxx 00, 0000.

Digital Object Identifier 10.1109/ACCESS.2024.0429000

Loss Analysis of Permanent Magnet Synchronous Motor System based on Strategy-Circuit-Field Co-Simulation and an Accurate Iron Loss Calculation Method

WEI LI[1], (Member, IEEE), JIANGFAN XUE[1], XING FAN[1], and LIXUN ZHU[2]

[1]Department of Electrical Engineering, Tongji University, Shanghai, 201804, China
[2]Department of Logistics Engineering, Shanghai Maritime University, Shanghai, 200135, China

Corresponding author: Jiangfan Xue (e-mail: xuejiangfan@tongji.edu.cn), and Lixun Zhu (e-mail: lixzhu@shmtu.edu.cn)

This work was supported in part by the National Natural Science Foundation of China under Grant 52007113 and Grant 52377014, and in part by the National Key Research and Development Program of China under Grant 2023YFB2504304 and 2023YFB2504300.

ABSTRACT With the development of permanent magnet synchronous motors (PMSMs), the accurate loss calculation is of vital significance for the performance evaluation of the PMSM system. As the loss of the PMSM system is determined by the control strategy, inverter, and the motor itself, which interact with each other mutually and complicatedly, in conventional loss calculation methods they are not considered synthetically. To calculate the PMSM system loss accurately, this paper proposes a strategy-circuit-field co-simulation methodology, which can take into account the mutual influence of control strategy, inverter, and motor. The proposed co-simulation platform synchronizes the control theory-based strategy simulation, Kirchhoff's law-based circuit simulation, and the field-based motor simulation, which reveals the real physical process of PMSM systems. To further improve the loss calculation accuracy, a hysteresis-based iron loss calculation method is introduced and utilized. The co-simulation results show that the proposed method can reflect the behavior of the PMSM system more physically, and mutual influence between the three aspects can be presented. Finally, the corresponding experiments are conducted, and the results are compared with the simulation results, proving the proposed methodology's feasibility and effectiveness.

INDEX TERMS Co-simulation, hysteresis-based iron loss model, loss calculation, permanent magnet synchronous motor (PMSM)

I. INTRODUCTION

PERMANENT magnet synchronous motors (PMSMs), known for their high performance, high efficiency, high power density, and excellent control capabilities, are now widely utilized in areas of new energy vehicles and robotics [1], [2]. In recent years, to improve product performance and enhance market competitiveness, PMSMs are rapidly developing towards higher speeds, higher efficiency, and wider constant power speed range [3], [4], [5]. For example, the PMSM in the automotive industry has currently achieved a speed up to 20000 rpm. When using PMSMs, it is necessary to cooperate with inverters to achieve speed regulation. With the increase of switching frequency, the losses of the inverter and motors are increasing. These losses are emitted in the form of heat, causing the temperature of the motor system to rise [6]. This not only leads to a decrease in product endurance but also poses a threat to the lifespan of the motor and the inverter. Owing to the switching behavior of power electronic devices and the magnetic material saturation of PMSMs, harmonics are generated in the system, thereby causing losses [7]. Hence, it is imperative to simultaneously consider all the factors to achieve a comprehensive and accurate assessment of the losses of PMSM systems.

The losses of the PMSM system driven by the inverter are mainly divided into inverter loss and motor loss [8]. The inverter loss is mainly caused by the power electronic devices during their conduction and switching processes. In high voltage and high current application scenarios, as the switching frequency increases with the increase of motor speed, the loss of IGBT modules will greatly increase, resulting in an increase in IGBT junction temperature. In severe cases, it may lead to IGBT failure, affecting the reliability and lifespan of

the inverter [9].

The losses generated on the motor mainly include copper losses, mechanical losses, iron losses, and permanent magnet loss [10] [11]. The copper loss of the motor is mainly caused by the Joule heat loss generated by the current flowing through the motor winding. As the frequency increases, the copper loss of the motor will gradually increase due to the influence of skin effect and proximity effect [12]. Mechanical loss is caused by friction between motor bearings, rotor wind resistance, and other factors [13]. When the motor rotates at high speed, the air friction on the rotor surface increases, resulting in an increase in mechanical loss [14]. In a very small rotor heat dissipation space, it can cause temperature rise and even demagnetize the permanent magnet [15]. Iron loss is caused by the movement of magnetic domain walls and eddy currents caused by the alternating main magnetic flux in the motor iron core, especially when the motor operates at high speed [16]. The high-speed alternating magnetic field can cause a rapid increase in iron loss, affecting the performance of the motor. The traditional loss separation method is relatively accurate for estimating iron loss under sinusoidal excitation. However, due to the nonlinearity of ferromagnetic materials and the introduction of a large number of harmonics into the motor by the inverter, the computational complexity of iron loss is greatly increased, and the accuracy is significantly reduced [17]. In this case, the hysteresis model of ferromagnetic materials must be considered, and iron loss calculation based on hysteresis models can be more accurate. Reference [18] proposed using experimental data combined with the LS hysteresis model to calculate iron loss and the accuracy is verified.

In order to analyze the PMSM losses accurately, a strategy-circuit-field co-simulation method is proposed in this paper. By adopting the co-simulation method, the magnetic field harmonics caused by the control strategy, inverter, and motor saturation can be taken into account when evaluating the losses mentioned above. Particularly, the iron loss of the PMSM is much influenced by the inverter harmonics. In order to calculate the iron loss accurately, an iron loss evaluation method based on the hysteresis model is adopted, which is capable of simulating the minor loops caused by inverter harmonics.

Firstly, the id=0 control strategy of PMSMs is introduced, based on which the mathematic model of PMSMs is replaced with Finite Element Method (FEM) model, and the strategy-circuit-field co-simulation platform is constructed. By setting the appropriate time step for each part of the platform, the simulation process among different packages can achieve real-time interaction and keep pace with each other. Compared with the results in separated simulations, the results of the co-simulation can reflect current and magnetic field harmonics, which is the basis for accurate loss calculation. Secondly, the theoretical and computational methods of various losses in the inverter-driven PMSMs are introduced, especially for the iron loss that is crucial and difficult to calculate accurately. The iron loss calculation method based on the LS hysteresis model is adopted to improve the accuracy of loss calculation. Subsequently, the co-simulations of the PMSM under different load conditions are performed, and various losses of the system are calculated separately. Finally, a PMSM experimental platform is established, and various losses of the PMSM during actual operation are measured. The experimental data verified the accuracy and effectiveness of the loss calculation method proposed in this paper.

II. STRATEGY-CIRCUIT-FIELD CO-SIMULATION

A. STRATEGY-CIRCUIT-FIELD SYNCHRONOUS SYSTEM

The commonly used control methods for PMSMs include id=0 control, maximum torque per ampere (MTPA) control, maximum efficiency per ampere (MEPA) control, direct torque control, etc [19], [20]. These control methods are generally based on the dynamic model of the motor. Fig.1 shows the block diagram of a PMSM speed control system using the id=0 control strategy. The speed loop and current loop are respectively controlled by PI regulators, and the modulation module is implemented by the SVPWM technique. Based on the control instructions, the expected stator voltage vector is calculated in the SVPWM module, and then the switching sequence of the six IGBT modules in the inverter is obtained. The PMSM is driven by the inverter and responds under the constraints of excitations and loads. Meanwhile, the electromagnetic parameters such as magnetic flux, current, and torque are fed back to the control system for calculation, achieving closed-loop control of the PMSM system.

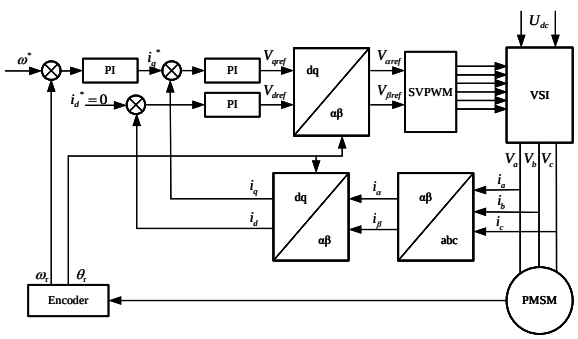

FIGURE 1. Id=0 Control Block Diagram.

In most scenarios, the idealized dynamic mathematic model of PMSM is adopted in the control system, which means that the inductance is assumed to be constant as shown in (1). As a result, the real physical aspects of the PMSM cannot be taken into account, such as the nonlinear property of materials and the magnetic field distribution.

$$\begin{cases} \psi_{\mathrm{d}} = L_{\mathrm{d}} i_{\mathrm{d}} + \psi_{\mathrm{f}} \\ \psi_{\mathrm{q}} = L_{\mathrm{q}} i_{\mathrm{q}} \end{cases} \tag{1}$$

where subscripts of flux linkage ψ, inductance L, and stator current i denote their corresponding dq components, while

ψ_f stands for the excitation magnetic flux of the permanent magnet of the rotor.

Yet the electromagnetic torque equation is related to the flux linkage as shown in (2). Once the magnetic flux is not reliable, the computed torque and the dynamic response of the motor would differ from the real motor, and then the calculation accuracy of motor losses would decrease.

$$T_e = \frac{3}{2} p_n \left(\psi_d i_q - \psi_q i_d \right) \tag{2}$$

where T_e is the electromagnetic torque of the PMSM and p_n is the number of pole pairs.

If the PMSM is modeled by FEM, the magnetic field can be calculated accurately, and the omitted aspects such as material saturation, leakage flux, and cross-coupling, can all be involved, and thus the flux linkage can be obtained accurately.

The PMSM supplied through the SVPWM technique contains lots of harmonics due to the high switching frequency. The losses including the iron loss, the copper loss, and the eddy current loss of PM, are influenced by the current and magnetic field harmonics, therefore, in order to acquire the exciting current precisely, it is necessary to combine the circuit simulation and the field computation.

This paper proposed a strategy-circuit-field co-simulation platform. The overall control logic diagram is shown in Fig.2. The control strategy is executed in the Simulink Package, which takes the motor speed and current as the feedback input quantities and outputs the switching sequence of the power electronic switches to the Simplorer package. The PMSM responds correspondingly with the circuit excitation and outputs the electromagnetic torque to the load, which are all simulated in the FEM package. The three packages should run at the same time step length, which ensures the real-time data exchange. The application of co-simulation allows for a balanced consideration of the impact of motor control strategies and the motor itself on system losses. Additionally, the use of co-simulation data for further calculations of iron losses will enhance accuracy.

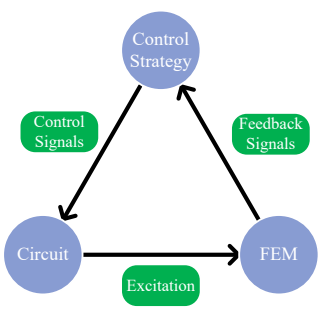

FIGURE 2. Co-simulation interaction diagram

B. RESULTS OF THE CO-SIMULATION

In the co-simulation, the motor speed is set to 3000 rpm and the load torque is 16 Nm. The time step is 1e-5 s and the total simulation time is 0.18s. By co-simulation, the speed, torque, phase current, d-q axis current, and the rotor position are all obtained and shown in Fig.3. The motor speed rises to 3000 rpm and remains stable. The motor torque is slightly high during the motor starting process but quickly decreases to match the load torque.

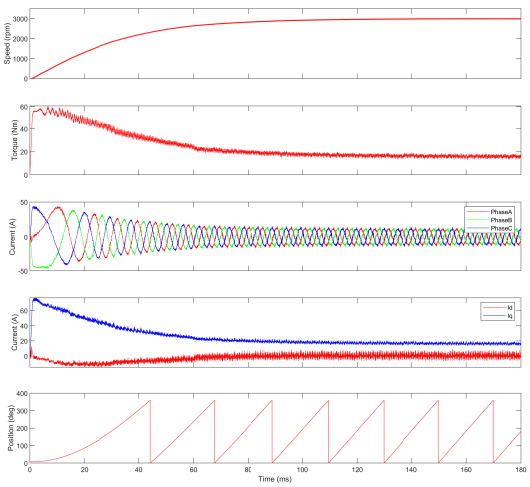

FIGURE 3. Waveforms of co-simulation results including speed, torque, phase currents, d-q axis currents and the rotor position.

In addition to the dynamic response data of the motor, the magnetic density cloud map of the motor can also be calculated as shown in Fig.4. The magnetic induction intensity in certain parts is relatively high, which may cause saturation of ferromagnetic materials.

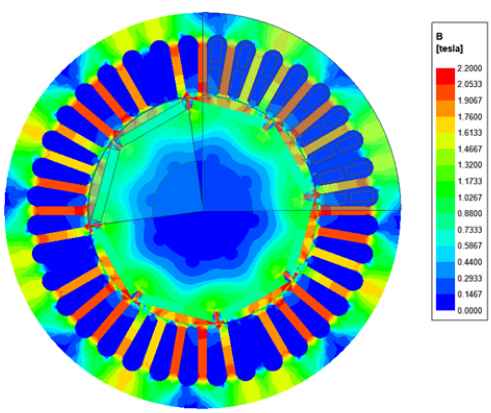

FIGURE 4. The magnetic density cloud map obtained from co-simulation

To study the transient response of the co-simulation platform, both co-simulation and separated simulation are con-

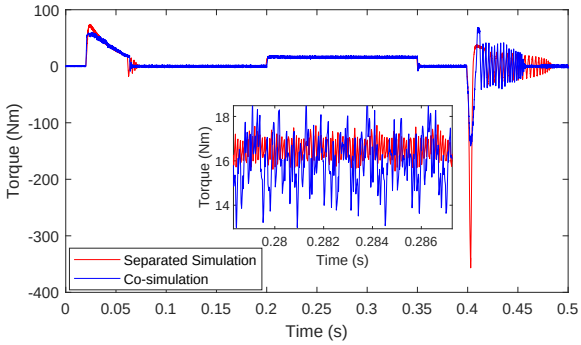

(a) The waveform of the motor torque

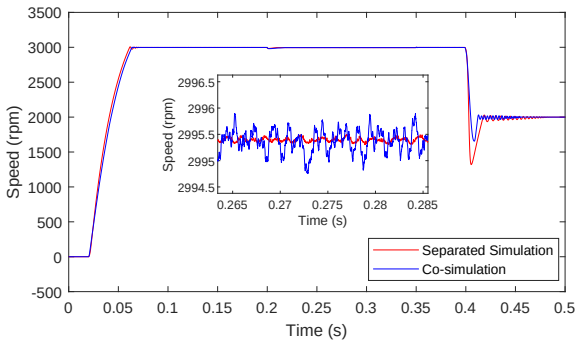

(b) The waveform of the motor speed

FIGURE 5. The waveform of the motor torque and speed calculated by separated simulation and co-simulation respectively.

ducted under four working states, including acceleration, loading, unloading, and deceleration.

First, the motor is started from 0 rpm to 3000 rpm at no load condition. Then, the load is increased to 16 Nm at 0.2 s, and at 0.35 s the load is reduced to 0 Nm. Finally, the motor speed is regulated to 2000 rpm. The motor torque and speed waveform are shown in Fig.5.

The steady-state results of both the separated simulation and co-simulation show consistent convergence in the above four stages. In the co-simulation, the internal electromagnetic field of the motor is calculated by FEM, and the effects of factors such as cogging torque, motor saturation, leakage flux, and armature reaction on the system can be considered. Therefore, the electromagnetic torque vibration in the steady state is also greater. Due to the difference in electromagnetic torque calculated by the analytical model in the separated simulation and the finite element model in the co-simulation, the dynamic response of the co-simulation differs from that of the separated simulation. The co-simulation is more stable in all the dynamic processes of the four working states.

Owing to the influence of PWM excitations and power electronic devices on the internal magnetic field of the motor, as well as the nonlinearity of the motor magnetic circuit, a large number of harmonics are introduced into the stator current of the motor. These factors can also be reflected in the waveform of the motor stator current shown in Fig.6. The introduction of stator current harmonics will cause an increase in motor iron loss, copper loss, etc. Therefore, adopting co-simulation to calculate motor system losses can approach real losses more closely.

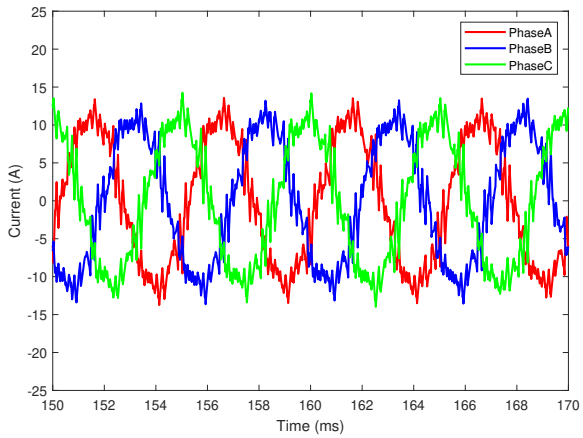

FIGURE 6. The stator current waveform calculated by co-simulation reflecting a large number of harmonics.

The Fourier analysis on the stator current of the motor obtained from co-simulation is performed, as shown in Fig.7. In addition to the higher amplitude distributed at the fundamental frequency, i.e. the operating frequency of the motor, there are also significant harmonic components at the switching frequency and its harmonics. Due to the correlation between the magnetic induction intensity and the magnetic field intensity, the behavior of motor ferromagnetic materials under the excitation containing high-order harmonics is more complicated than that under sine wave excitations, resulting in inconsistency in motor iron loss, eddy current loss, etc.

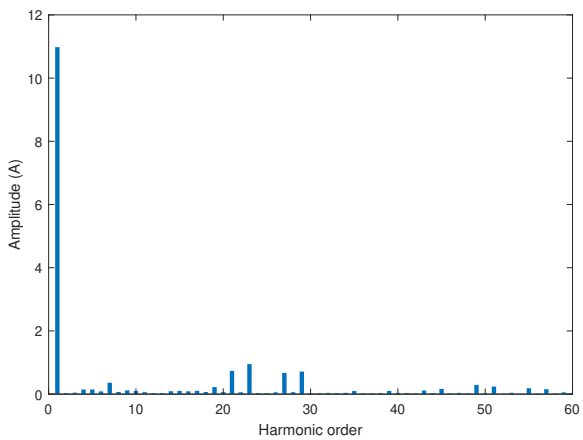

FIGURE 7. Phase current spectrum distribution diagram

In order to study the impact of inverter power supply on the motor, four points at different positions of the motor stator, including tooth top, tooth center, tooth root, and tooth yoke are selected, and the magnetic loci are observed, as depicted in Fig.8 and Fig.9. In contrast to the sine wave excitation, the magnetic induction intensity waveform under

SVPWM control exhibits numerous harmonics, which will lead to additional iron loss.

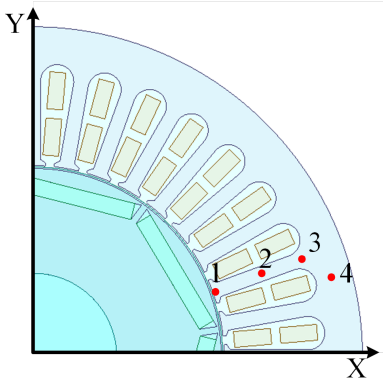

FIGURE 8. Schematic diagram of motor stator characteristic points

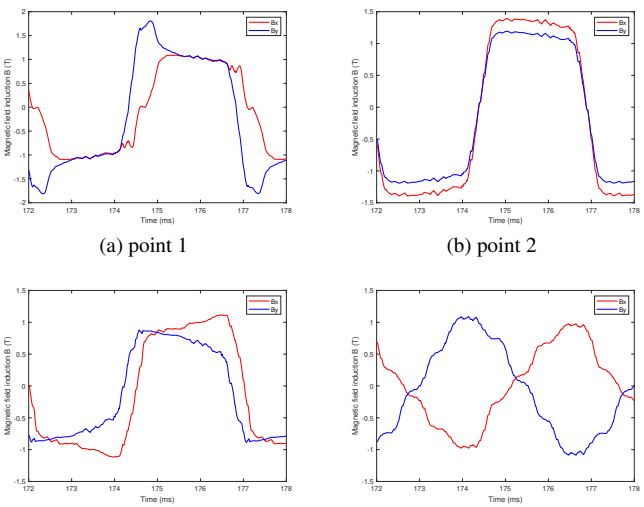

(a) point 1 (b) point 2

(c) point 3 (d) point 4

FIGURE 9. Magnetic induction intensity waveforms at different points

III. LOSS CALCULATION OF PMSM SYSTEM

The proposed loss calculation schematic diagram based on the co-simulation platform is shown in Fig.10. The total loss of the PMSM system mainly includes losses on the inverter side and losses on the motor side. The inverter side loss mainly concerns the loss of the IGBT module. The motor side losses mainly include the copper loss, the iron loss, the eddy current loss of permanent magnets, and the mechanical loss. All the losses are further calculated based on the obtained co-simulation results.

A. CALCULATION OF THE IGBT LOSS

The losses of the inverter are mainly reflected in the IGBT modules, which are composed of IGBT and the freewheeling diode (FWD). The loss calculation methods of IGBT modules can be divided into physical modeling method and formula

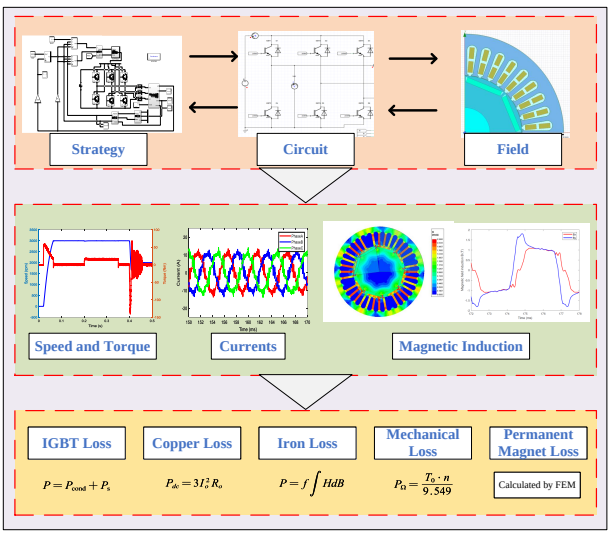

FIGURE 10. Co-simulation and loss calculation schematic diagram

derivation method. The physical modeling method refers to establishing a model of an IGBT, simulating its transient voltage and current characteristics, and then calculating its loss. The formula derivation method is to derive and calculate the loss of IGBT modules based on control theory, power electronics technology, and other theories. These two methods cannot take into account the motor state during the operation of the inverter. This paper adopts the method of combining the co-simulation platform with the formula derivation method to calculate the loss of IGBT modules [21]. The power loss caused by the conduction voltage drop of IGBT modules is called conduction loss. The conduction loss of IGBT and FWD when outputting sine waves can be obtained by (3) and (4).

$$\begin{aligned} P_{\mathrm{cond\_Tr}} =& I_{\mathrm{out}}\sqrt{2}\left(\frac{1}{2\pi}+\frac{M\cos\varphi}{8}\right)[V_{\mathrm{Tr\_25^\circ C}}+ \\ & K_{\mathrm{v\_Tr}}\left(T_{\mathrm{j}}-25^\circ\mathrm{C}\right)]+I_{out}^2 2\left(\frac{1}{8}+\frac{M\cos\varphi}{3\pi}\right) \\ & [r_{\mathrm{Tr\_25^\circ C}}+K_{\mathrm{r\_Tr}}\left(T_{\mathrm{j}}-25^\circ\mathrm{C}\right)] \end{aligned} \tag{3}$$

$$\begin{aligned} P_{\mathrm{cond\_D}} =& I_{\mathrm{out}}\sqrt{2}\left(\frac{1}{2\pi}-\frac{M\cos\varphi}{8}\right)[V_{\mathrm{D\_25^\circ C}}+ \\ & K_{\mathrm{v\_D}}\left(T_{\mathrm{j}}-25^\circ\mathrm{C}\right)]+I_{\mathrm{out}}^2 2\left(\frac{1}{8}-\frac{M\cos\varphi}{3\pi}\right) \\ & [r_{\mathrm{D\_25^\circ C}}+K_{\mathrm{r\_D}}\left(T_{\mathrm{j}}-25^\circ\mathrm{C}\right)] \end{aligned} \tag{4}$$

where $P_{\mathrm{cond\_Tr}}$ and cond_D are the conduction loss of the IGBT and the FWD respectively, I_{out} is the RMS value of the current, M is the modulation ratio of PWM, φ is the power factor angle, $V_{\mathrm{Tr\_25^\circ C}}$ and $V_{\mathrm{D\_25^\circ C}}$ are the actual conduction voltage drop of the IGBT and the FWD at 25°C respectively, $K_{\mathrm{v\_Tr}}$ and $K_{\mathrm{v\_D}}$ are the coefficient of the effect of temperature on the conduction voltage drop of IGBT and FWD

respectively, $r_{\mathrm{Tr\_25^\circ C}}$ and $r_{\mathrm{D\_25^\circ C}}$ are the on-state resistance of the IGBT and the FWD respectively, $K_{\mathrm{r\_Tr}}$ and $K_{\mathrm{r\_D}}$ are the coefficient of the effect of temperature on the on-state resistance of IGBT and FWD respectively, T_j is the actual junction temperature of the IGBT module.

Besides the conduction loss, the loss of IGBT and FWD during each switching cycle can be calculated by (5) and (6).

$$P_{\mathrm{s\_Tr}} = f_{\mathrm{s}} \left(E_{\mathrm{on}} + E_{\mathrm{off}}\right) \frac{\sqrt{2}}{\pi} \left(\frac{I_{\mathrm{out}}}{I_{\mathrm{rated}}}\right)^{K_{\mathrm{sTrI}}} \left(\frac{V_{CC}}{V_{\mathrm{rated}}}\right)^{K_{\mathrm{sTrV}}} \left[1 + K_{\mathrm{sTrT}} \left(125^\circ\mathrm{C} - T_{\mathrm{j\_Tr}}\right)\right] \tag{5}$$

$$P_{\mathrm{s\_D}} = f_{\mathrm{s}} E_{\mathrm{rr}} \frac{\sqrt{2}}{\pi} \left(\frac{I_{\mathrm{out}}}{I_{\mathrm{rated}}}\right)^{K_{\mathrm{sDI}}} \left(\frac{V_{\mathrm{CC}}}{V_{\mathrm{rated}}}\right)^{K_{\mathrm{sDV}}} \left[1 + K_{\mathrm{sDT}} \left(125^\circ\mathrm{C} - T_{\mathrm{j\_D}}\right)\right] \tag{6}$$

where $P_{\mathrm{s\_Tr}}$ and $P_{\mathrm{s\_D}}$ are the switching loss of the IGBT and the FWD respectively, f_s is the carrier frequency, E_{on} and E_{off} are the single pulse turn-on and turn-off loss, E_{rr} is the single pulse turn-off loss of the FWD, I_{rated} and V_{rated} are the rated current and voltage, K_{sTrI} and K_{sDI} are the coefficient of the effect of current amplitude on the switching loss of IGBT and FWD respectively, K_{sTrV} and K_{sDV} are the coefficient of the effect of voltage amplitude on the switching loss of IGBT and FWD respectively, K_{sTrT} and K_{sDT} are the coefficient of the effect of temperature on the switching loss of IGBT and FWD respectively.

A two-level inverter has 6 IGBT modules, while each module has its own conduction loss and switching loss for the IGBT and FWD. Therefore, the loss of the inverter is the sum of the loss of the 6 modules as (7).

$$P = 6\left(P_{\mathrm{cond\_Tr}} + P_{\mathrm{cond\_D}} + P_{\mathrm{s\_Tr}} + P_{\mathrm{s\_D}}\right) \tag{7}$$

B. CALCULATION OF THE IRON LOSS

The iron loss of a motor is reflected in the hysteresis loop of the material. If the distribution of the motor hysteresis loop can be accurately calculated, the iron loss can be accurately calculated. This paper adopts the iron loss calculation method based on the LS hysteresis model, which can be used for accurate calculation of motor iron loss under harmonic excitation [18]. In the LS hysteresis model, the magnitude of magnetic field intensity is related to the magnitude, rate of change, and amplitude of magnetic induction intensity. As shown in (8),

$$H = f\left(dB/dt, B, B_m\right) \tag{8}$$

where H is the magnetic field intensity, B is the magnetic induction intensity, B_m is the amplitude of the magnetic induction intensity, and dB/dt is the rate of change of the magnetic induction intensity.

By measuring the magnetic field strength of ferromagnetic materials at different magnitudes and rates of magnetic induction, an LS hysteresis model database of ferromagnetic materials in motors can be extracted, as shown in Fig.11.

The LS hysteresis model can compute the magnetic field strength at any magnetic induction intensity. The hysteresis

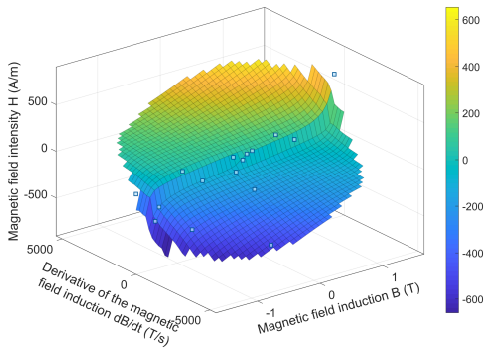

FIGURE 11. Loss Surface of the ferromagnetic material used in the tested motor

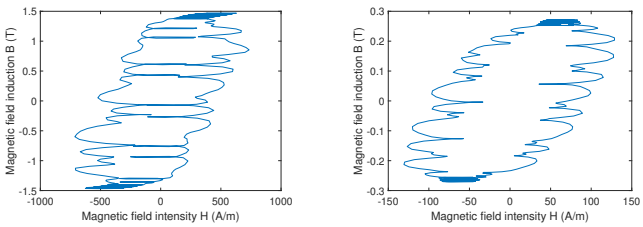

(a) the tooth root (b) the tooth center

FIGURE 12. Hysteresis loop at the studied tooth root and the tooth center.

loop corresponding to the tooth root and the tooth positions is shown in Fig.12. Due to the influence of harmonic excitation, the hysteresis loop contains many local hysteresis loops, which will increase the iron loss.

Through the built co-simulation platform, it is possible to simulate the operating status of the motor under different working conditions. The magnetic induction intensity waveform of each element can be obtained. Combined with the established LS hysteresis model database, the hysteresis loop of the material can be fitted. The iron loss of each element is calculated as shown in (9).

$$P = f \int HdB \tag{9}$$

where f is the frequency of magnetic induction intensity. By summing up the iron losses of all elements, the total iron loss of the entire motor can be obtained.

C. CALCULATION OF COPPER LOSS

The copper loss of the motor is mainly caused by the alternating current flowing through the motor winding. Due to the influence of the skin effect and proximity effect, the effective area of the conductor decreases, and the equivalent resistance increases, leading to an increase in winding losses. The AC copper loss of motor windings mainly includes DC loss and eddy current loss, which can be represented as the following equation.

$$P_{ac} = P_{dc} + P_{eddy} \tag{10}$$

where P_{ac} is the AC copper loss of the winding, P_{dc} is the DC loss of the winding, and P_{eddy} is the eddy current loss of the winding. The DC loss of three-phase PMSM can be calculated by the following equation (11)

$$P_{dc} = 3I_o^2 R_o \tag{11}$$

where I_o is the phase current of the motor, R_o is the phase resistance of the motor. The total copper loss including the eddy current loss can also be calculated accurately by using FEM.

D. CALCULATION OF THE PERMANENT MAGNET LOSS

Due to the relatively low electrical resistivity of the permanent magnet materials used in PMSMs, large eddy currents will be induced in the permanent magnet in high-frequency alternating electromagnetic fields, causing permanent magnet loss. The eddy current loss of permanent magnets is related to the changes in magnetic field, permanent magnet materials, and permanent magnet structure. In the inverter-driven PMSM system, a large number of harmonics will be introduced into the motor current, which will also greatly increase the eddy current loss of the permanent magnet. For inner rotor PMSMs, the heat dissipation conditions of the permanent magnet are poor. As the eddy current loss of the permanent magnet increases, the temperature of the permanent magnet will continue to rise, and even lead to demagnetization of the permanent magnet, affecting the reliability and stability of the motor. The eddy current loss of permanent magnets is not easy to be measured directly through experiments, and FEM can generally be adopted for calculation.

E. CALCULATION OF THE MECHANICAL LOSS

The mechanical loss mainly includes the bearing friction loss and the ventilation loss. Among them, the friction loss of bearings is related to the smoothness of the friction surface, the type of lubricating oil, working temperature, etc., and the friction coefficient is relatively difficult to determine. Meanwhile, ventilation loss is related to motor structure, fan type, ventilation system wind resistance, etc., and is difficult to accurately calculate. Therefore, mechanical loss is often obtained through motor experiments. This paper customizes a motor with the same rotor size and structure as the tested motor, but without magnetization, namely a fake rotor motor. The fake rotor motor is driven by an induction motor, and the mechanical output power of the induction motor is the mechanical loss of the tested motor, which is determined by (12).

$$P_{\Omega} = \frac{T_0 \cdot n}{9.549} \tag{12}$$

where T_0 is the output torque of the induction motor and n is the speed of the induction motor. By measuring the loss at different speeds, the mechanical loss curve can be obtained.

IV. LOSS CALCULATION RESULTS OF THE PMSM SYSTEM

A PMSM with a rated power of 5.5kW is studied in this paper, and the detailed motor parameters are shown in Table.1. The PMSM system is simulated by adopting the proposed co-simulation platform, and the various losses are calculated by using the corresponding proposed methods, respectively.

TABLE 1. The Detailed Parameters of the PMSM

Parameter (unit)	Value
Rated Power (kW)	5.5
Rated Current (A)	10
Rated Frequency (rpm)	200
Rated Torque (Nm)	16
Number of Pole-pairs	4
Length of Cores (mm)	60
Outer Diameter of Stator (mm)	181
Inner Diameter of Stator (mm)	105
Number of Stator Slots	36
Core Material	DW465-50

By calculating the copper losses at different speeds and load torques, the copper loss distribution is shown in Fig.13. The copper loss of the motor increases gradually with the increase of torque. That is, compared to the speed, the copper loss of the motor is more affected by torque.

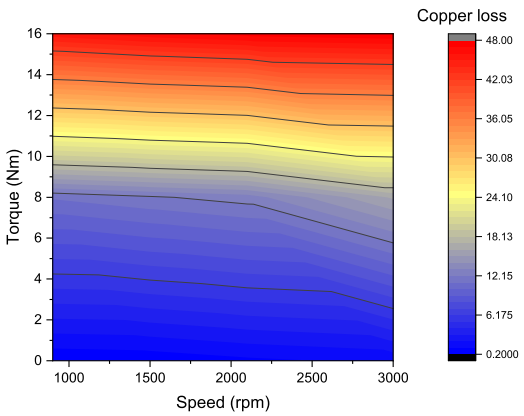

FIGURE 13. Copper loss under different operating conditions

The iron loss under different operating conditions is shown in Fig.14. It reveals that the iron loss is related more to the motor speed. As the motor speed increases, the frequency of the magnetic field accelerates as well, amplifying hysteresis and eddy current effects in the iron core, which, in turn, enhances the iron loss. Besides, the iron loss of the motor does increase slightly with the increase of torque, but this increase is actually not significant compared to the total iron loss of the motor. Therefore, the result in Fig.14 shows that the iron loss does not change much with the torque.The permanent magnet loss is shown in Fig.15. As the eddy current loss of permanent magnets is related to magnetic field strength and alternating frequency, the eddy current loss of permanent magnets will also increase as the motor speed and torque increase.

By adding up the various losses of the motor under different operating conditions, the total loss of the motor under different operating conditions can be obtained, as shown in

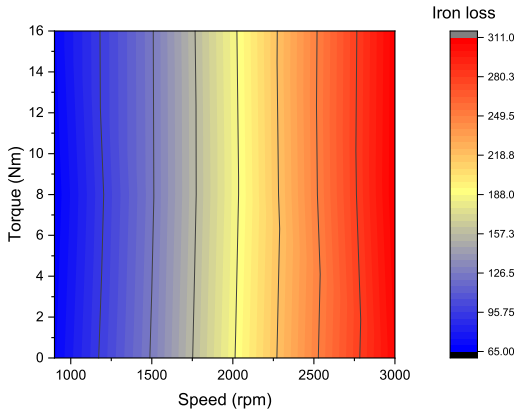

FIGURE 14. Iron loss under different operating conditions

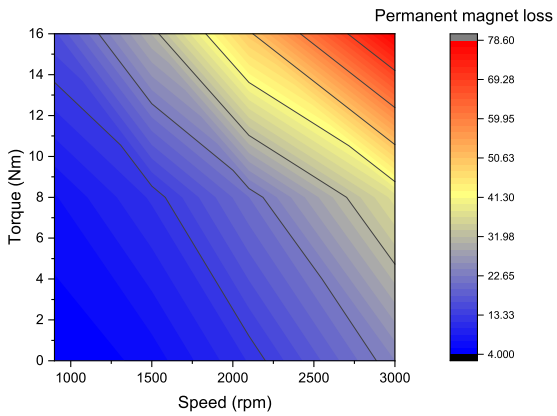

FIGURE 15. Permanent magnet loss under different operating conditions

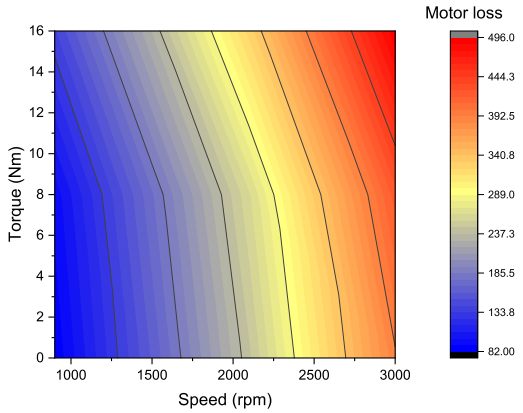

FIGURE 16. Motor loss under different operating conditions

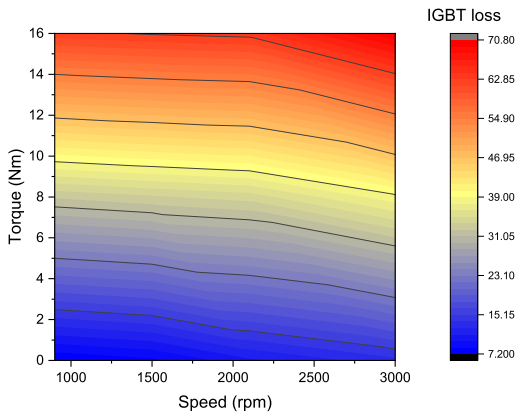

FIGURE 17. IGBT loss under different operating conditions

Fig.16. As the motor speed and load increase, the total loss also gradually increases.

The loss of the inverter under different operating conditions is shown in Fig.17. As the current increases with the increase of load torque, the loss of the inverter will also increase.

Based on the above calculations, the total loss of the inverter-driven PMSM system can be obtained, as shown in Fig.18. The loss value increases with the increase of speed and torque. The determination of system loss is also of great reference significance for the new energy vehicles.

V. EXPERIMENTAL VERIFICATIONS

In order to verify the accuracy of the method proposed in this paper, experimental measurements are conducted on a 5.5kW PMSM. The losses generated in the PMSM mainly include copper loss P_{Cu}, iron loss P_{Fe}, mechanical loss P_{Ω}, and permanent magnet loss P_{mag}, as shown in Fig.19.

The total loss of the PMSM is obtained by subtracting the output power P_{out} from the input power P_{in}. Comparing the

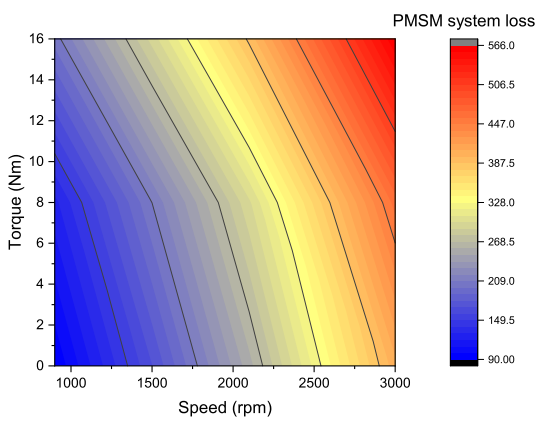

FIGURE 18. Motor system loss under different operating conditions

calculated loss with the actual loss of the PMSM, the graph shown in Fig.20 can be obtained. The result shows that the

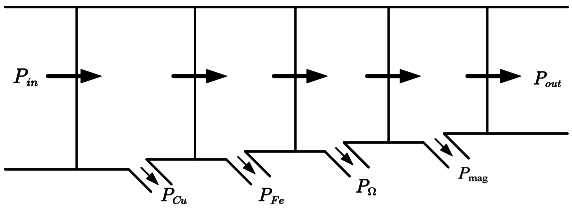

FIGURE 19. Distribution diagram of motor loss

calculated loss by the proposed method matches well with the measured loss.

Besides the PMSM loss, the iron loss in the system is also obtained through experiments. Since the iron loss is not very easy to measure directly, the principle of energy conservation is introduced to calculate the actual iron loss as (13).

$$P_{Fe} = P_{in} - P_{Cu} - P_{\Omega} - P_{\mathrm{mag}} - P_{out} \tag{13}$$

among which the copper loss is obtained by measuring the motor phase resistance and phase current at different speeds. Meanwhile, the fake rotor method is used to measure the mechanical loss of the motor at different speeds. A motor towing platform is constructed in the experiment as shown in Fig.21. The left side of the platform is the PMSM to be tested, and the right side is the dragging motor. The two motors are connected through couplings and speed torque sensors. The measured mechanical loss is shown in Table.2. It should be emphasized that due to the difficulty in measuring the PM loss, the PM loss is replaced with the data obtained from finite element software under corresponding operating conditions.

The calculation results of the iron loss at different frequencies and loads are compared with the experimental results, as shown in Table.3. The result shows that the error between the calculated iron loss and the experimental iron loss is within a reasonable range compared with the conventional loss separation methods.

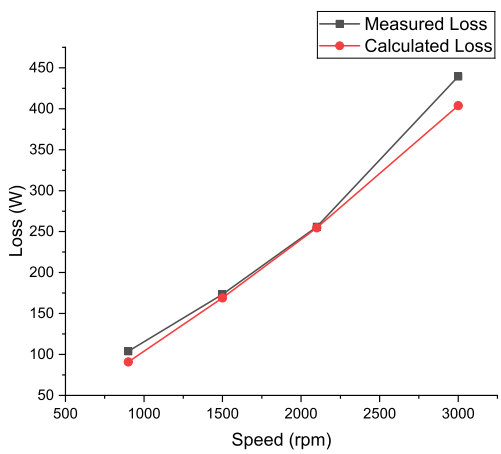

FIGURE 20. Comparison between calculated system loss and measured system loss

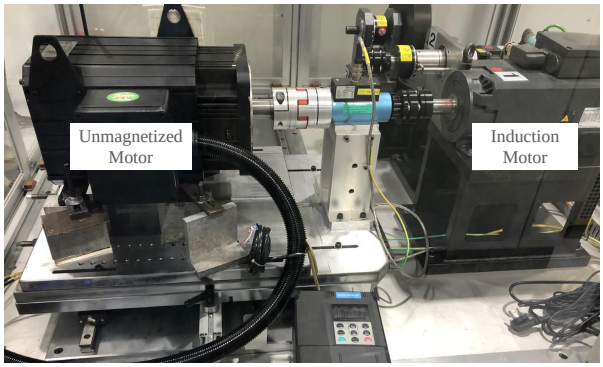

FIGURE 21. Experimental platform

TABLE 2. The measured mechanical loss at different frequencies

Frequency (Hz)	Mechanical loss (W)
60	9.9
100	26.6
140	32.8
200	58.4

TABLE 3. The measured and calculated iron Loss at different frequencies and loads

Frequency (Hz)	Load (Nm)	Measured iron loss (W)	Calculated iron loss (W)	Error
60	0	67.8	69.2	2.01%
60	8	68.4	65.9	-3.65%
60	16	85.3	69.6	-18.39%
100	0	113.9	127.6	12.0%
100	8	119.6	124.9	4.45%
100	16	135.6	125.4	-7.5%
140	0	211.5	198.1	6.3%
200	0	366.0	306.2	16.3%

VI. CONCLUSION

This paper proposed a loss analysis methodology of inverter-driven PMSM systems based on a physical fact approached co-simulation strategy. Harmonics is the principal aspect of the research, which directly determines the applicability of the loss calculation methodology, especially for iron loss. By adopting the proposed strategy-circuit-field co-simulation platform, the harmonics in the PMSM system can be presented. Therefore, different loss calculation methodologies can be applied to the corresponding scenarios. The loss calculation accuracy is verified by various experimental tests, which shows the feasibility of the proposed method. The proposed analysis method does not rely on experiments, which gives more application opportunities. The loss distribution of the PMSM system at concerned operating conditions can all

be obtained. The proposed methodology can also be applied to other harmonic-involved electric machine systems.

REFERENCES

[1] M. Li, H. Tan, H. Cai, Y. Gao, Y. Li, and S. Li, "Online maximum efficiency control based on mras for unmanned air vehicle surface-mounted high-speed pmsm," in *2017 Chinese Automation Congress (CAC)*, 2017, pp. 5812–5817.

[2] A. Yang, M. Lin, L. Jia, and K. Lin, "A modified rotor flux observer based sensorless method for dual three-phase pmsm," in *2023 IEEE International Conference on Applied Superconductivity and Electromagnetic Devices (ASEMD)*, 2023, pp. 1–2.

[3] H. Kumar, M. R. Dhanvijay, R. Maravulla, and S. M. Patil, "An overview of efficiency improvement strategies for electric vehicle drivetrain using pmsm drives to mitigate ev range anxiety," in *2022 International Conference on Innovations in Science and Technology for Sustainable Development (ICISTSD)*, 2022, pp. 24–29.

[4] L. Zhu, Q. Wu, W. Li, W. Wu, C.-S. Koh, and F. Blaabjerg, "A novel consequent-pole magnetic lead screw and its 3-d analytical model with experimental verification for wave energy conversion," *IEEE Transactions on Energy Conversion*, vol. 39, no. 2, pp. 1202–1215, 2024.

[5] M. Li, S. Huang, X. Wu, K. Liu, X. Peng, and G. Liang, "A virtual hf signal injection based maximum efficiency per ampere tracking control for ipmsm drive," *IEEE Transactions on Power Electronics*, vol. 35, no. 6, pp. 6102–6113, 2020.

[6] X. Liu, G. Liu, and B. Han, "A Loss Separation Method of a High-Speed Magnetic Levitated PMSM Based on Drag System Experiment Without Torque Meter," *IEEE Transactions on Industrial Electronics*, vol. 66, no. 4, pp. 2976–2986, Apr. 2019.

[7] G. Feng, C. Lai, W. Li, Z. Li, and N. C. Kar, "Efficient Permanent Magnet Temperature Modeling and Estimation for Dual Three-Phase PMSM Considering Inverter Nonlinearity," *IEEE Transactions on Power Electronics*, vol. 35, no. 7, pp. 7328–7340, Jul. 2020.

[8] X. Ding, G. Liu, M. Du, H. Guo, C. Duan, and H. Qian, "Efficiency Improvement of Overall PMSM-Inverter System Based on Artificial Bee Colony Algorithm Under Full Power Range," *IEEE Transactions on Magnetics*, vol. 52, no. 7, pp. 1–4, Jul. 2016.

[9] A. M. Bazzi, P. T. Krein, J. W. Kimball, and K. Kepley, "IGBT and Diode Loss Estimation Under Hysteresis Switching," *IEEE Transactions on Power Electronics*, vol. 27, no. 3, pp. 1044–1048, Mar. 2012.

[10] P. Yulong, L. Xing, L. Yi, and C. Feng, "Effect of air gap eccentricity on rotor eddy current loss in high speed pmsm used in fess," in *2014 17th International Symposium on Electromagnetic Launch Technology*, 2014, pp. 1–6.

[11] M. Ciampolini, L. Fazzini, L. Berzi, G. Ferrara, and L. Pugi, "Simplified Approach for Developing Efficiency Maps of High-Speed PMSM Machines for Use in EAT Systems Starting from Single-Point Data," in *2020 IEEE International Conference on Environment and Electrical Engineering and 2020 IEEE Industrial and Commercial Power Systems Europe (EEEIC / I&CPS Europe)*, Jun. 2020, pp. 1–6.

[12] W. Yu, W. Hua, Z. Zhang, Z. Wu, P. Wang, and W. Xia, "Comparative Analysis of AC Copper Loss With Round Copper Wire and Flat Copper Wire of High-Speed Stator-PM Flux-Switching Machine," *IEEE Transactions on Industry Applications*, vol. 58, no. 6, pp. 7131–7142, Nov. 2022.

[13] S.-H. Park, E.-C. Lee, J.-C. Park, S.-W. Hwang, and M.-S. Lim, "Prediction of Mechanical Loss for High-Power-Density PMSM Considering Eddy Current Loss of PMs and Conductors," *IEEE Transactions on Magnetics*, vol. 57, no. 2, pp. 1–5, Feb. 2021.

[14] X. Su, H. Zhao, and F. Li, "Multiphysics research and loss calculation considering the fluid regime of the airgap based on high-speed pmsm," in *2023 26th International Conference on Electrical Machines and Systems (ICEMS)*, 2023, pp. 1885–1888.

[15] Y. Wan, S. Wu, and S. Cui, "Choice of Pole Spacer Materials for a High-Speed PMSM Based on the Temperature Rise and Thermal Stress," *IEEE Transactions on Applied Superconductivity*, vol. 26, no. 7, pp. 1–5, Oct. 2016.

[16] N. Boubaker, D. Matt, P. Enrici, F. Nierlich, and G. Durand, "Measurements of Iron Loss in PMSM Stator Cores Based on CoFe and SiFe Lamination Sheets and Stemmed From Different Manufacturing Processes," *IEEE Transactions on Magnetics*, vol. 55, no. 1, pp. 1–9, Jan. 2019.

[17] S. Steentjes, G. von Pfingsten, M. Hombitzer, and K. Hameyer, "Iron-Loss Model With Consideration of Minor Loops Applied to FE-Simulations of Electrical Machines," *IEEE Transactions on Magnetics*, vol. 49, no. 7, pp. 3945–3948, Jul. 2013.

[18] W. Li, X. Fan, L. Zhu, and C. Wei, "A Dynamic Hysteresis-Based Iron Loss Calculation Method and Its Application in a PWM-Fed IPMSM," *IEEE Transactions on Energy Conversion*, pp. 1–12, 2024.

[19] R. Ni, D. Xu, G. Wang, L. Ding, G. Zhang, and L. Qu, "Maximum efficiency per ampere control of permanent-magnet synchronous machines," *IEEE Transactions on Industrial Electronics*, vol. 62, no. 4, pp. 2135–2143, 2015.

[20] Y. Zhou and G. Chen, "Predictive dtc strategy with fault-tolerant function for six-phase and three-phase pmsm series-connected drive system," *IEEE Transactions on Industrial Electronics*, vol. 65, no. 11, pp. 9101–9112, 2018.

[21] J. Hu, J. Li, J. Zou, and J. Tan, "Losses calculation of IGBT module and heat dissipation system design of inverters," *Transactions of China Electrotechnical Society*, vol. 24, pp. 159–163, Mar. 2009.

WEI LI was born in Suihua, China. She received her B.S. and M.S. degrees in electrical engineering from Harbin Institute of Technology, Harbin, China, in 2005 and 2007, respectively. She received her Ph. D. degree in electrical engineering from Chungbuk National University, Chungbuk, Korea, in 2011.

She has been an assistant professor in the School of Electronics and Information Engineering, at Tongji University, Shanghai, China, since 2012. She is now an associate professor at Tongji University. Her current research interests include hysteresis modeling, finite element methods, and electric machines.

JIANGFAN XUE was born in Yuncheng, China. He received his B.S. degree from Tongji University, Shanghai, China, in 2022, where he is currently pursuing an M.S. degree in electrical engineering.

His research interests include electromagnetic field analysis, iron loss calculation, and high-performance AC motor drives.

XING FAN was born in Heze, China, in May 1999. She received her B.S. degree from Tongji University, Shanghai, China, in 2020, and is currently working toward a Ph.D. degree at the School of Electronics and Information Engineering, Tongji University, Shanghai, China.

Her current research interests include electromagnetic fields analysis, hysteresis modeling, and iron loss calculation.

LIXUN ZHU was born in Baotou, China. He received his Ph.D. degree in electrical engineering from Chungbuk National University, Korea in 2018.

He is currently an associate professor in the department of electrical engineering at Shanghai Maritime University, China. His research interests include renewable energy systems, motor design, and iron loss modeling. His research has been supported by the National Natural Science Foundation of China, and the Shanghai Science and Technology Innovation Action Plan.